Nonequilibrium Forces between Dragged Ultrasoft Colloids

Sunil P. Singh, Roland G. Winkler, and Gerhard Gompper

Theoretical Soft Matter and Biophysics, Institute for Advanced Simulation and Institute of Complex Systems, Forschungszentrum Jülich, D-52425 Jülich, Germany

(Received 3 August 2011; published 6 October 2011)

The dynamical deformation of ultrasoft colloids as well as their dynamic frictional forces are numerically investigated, when one colloid is dragged past another at constant velocity. Hydrodynamic interactions are captured by a particle-based mesoscopic simulation method. At vanishing relative velocity, the equilibrium repulsive force-distance curve is obtained. At large drag velocities, in contrast, we find an apparent attractive force for departing colloids along the dragging direction. The deformation, in the close encounter of colloids, and the energy dissipation are examined as a function of the drag velocity and their separation.

DOI: 10.1103/PhysRevLett.107.158301 PACS numbers: 83.80.Rs, 47.11.Mn, 82.35.Lr, 83.50.−v

Friction between macroscopic bodies has been studied for centuries. More recently, the microscopic processes responsible for friction and lubrication have come into focus, and have received broad attention [1–3]. Much less is known, however, about the nonequilibrium behavior of two mesoscopic, deformable particles sliding past each other under the effect of external forces. Such particles are ubiquitous in complex fluids and biofluids; droplets, capsules, vesicles, ultrasoft colloids and polymers are able to undergo large shape changes and have relaxation times comparable to the time scale of external perturbations [4–8]. Hence, (dense) suspension of such objects exhibit a much more complex nonequilibrium behavior than Newtonian liquids [9–11]. This is reflected, for example, in the formation of shear bands when a suspension is exposed to shear flow [12].

We focus here on the (time-dependent) friction between individual star polymers. Star polymers, which are composed of linear polymers linked to a common center by one of their ends, are particularly interesting because their properties can almost continuously be changed from that of flexible linear polymers to a spherical colloidal particle with very soft pair interactions [10–14]. Moreover, using synthetic and/or biopolymers, the size of the colloids can be varied from a few nanometers to micrometers [8]. This renders them interesting candidates for applications as lubricants, *inter alia*, in synovial joints.

Friction between mesoscopic particles, and thereby their rheological behavior, is determined by a broad range of forces on the nanoscale [15]. These include typical colloidal forces such as depletion, hydrodynamic drag, and lubrication forces [1,16]; for star polymers, elastic and entropic forces due to interactions and conformational changes on the atomistic scale are equally important.

In this Letter, we present mesoscale hydrodynamic computer simulation results of the nonequilibrium, nonstationary properties of strongly interacting star polymers in solution during dragging of two star polymers past each other at constant velocity. Our studies provide insight into the appearing universal nonequilibrium effective friction forces and structural changes. In particular, we show that on departure polymer repulsion turns into attraction at larger drag velocities. This behavior can be traced back to the retardation of polymer relaxation and symmetry breaking of the polymer conformations relative to the midplane between the polymer centers.

The dynamical response of star polymers crucially depends on the ratio of the relaxation time τ_r of a star, which is essentially determined by the relaxation time of a polymer arm, and the time set by the external motion, which we characterize by the time τ_d necessary to move one radius of gyration R_g of a star with the drag velocity v_d, i.e., $\tau_d = R_g/v_d$. We observe strong memory effects for $\tau_d < \tau_r$, since the system is not able to relax back to its equilibrium structure in this regime.

A hybrid mesoscale simulation approach is adopted, combining molecular dynamics simulations for polymers with the multiparticle collision dynamics (MPC) method for the solvent [17–19]. The consecutive monomers of the f polymer chains are connected by harmonic springs of bond length b. Excluded volume interactions are modeled by a repulsive Lennard-Jones potential with the parameter σ characterizing the monomer size and ϵ the energy [20]. Because of the high monomer concentration in the center, the diameter of the center bead and its bond lengths to next neighbors are twice that of other monomers. In the MPC method, the solvent is modeled by point particles, which undergo streaming and collision steps [17–20]. In the streaming step, the particles of mass m move ballistically for a time interval h. In the collision step, they, together with the monomers, are sorted into cubic cells of linear dimension a. Their relative velocities, with respect to the center-of-mass velocity of a cell, are rotated around a randomly oriented axis by an angle α. Temperature is kept constant by a local thermostat [20]. We adopted the parameters $\alpha = 130°$, $h = 0.1\sqrt{ma^2/k_BT}$, where k_B is

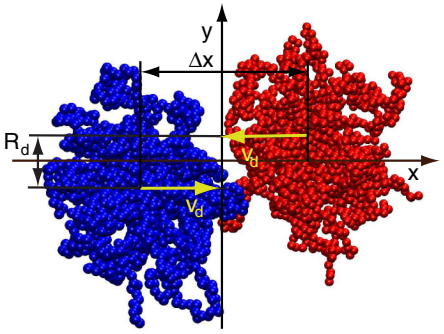

FIG. 1 (color online). Snapshot of stars dragged with constant velocity v_d and separated by R_d. See also movies S1 and S2 in the Supplemental Material [23].

Boltzmann's constant and T the temperature, the mean number of particles per cell $N_c = 10$, the monomer mass $M = 10m$, $b = a$, $\sigma = 0.8a$, $k_BT/\epsilon = 1$, and the system size $80a \times 60a \times 60a$ [20]. Stars are considered with $f = 20$, 40, and 60 arms of $N_m = 40$ monomers each. The central beads of the stars are confined in steep harmonic potentials at the positions $\boldsymbol{R} = (\mp v_d t, \pm R_d/2, 0)^T$, which corresponds to dragging with constant velocity v_d in time t (cf. Figure 1). We characterize the influence of the external force on the conformations of the stars by the Peclet number $\mathrm{Pe} = \tau_r/\tau_d = v_d\tau_r/R_g$, with the polymer relaxation time $\tau_r = \eta b^3 N_m^2/(k_BT) \approx 14\,000\sqrt{ma^2/k_BT}$; η is the solvent viscosity [21].

At equilibrium, the stars exert a repulsive force $\boldsymbol{F}$ on each other, which can be derived from the soft interaction potential of Refs. [13,14]. The bottom curve of Fig. 2 represents the equilibrium curve obtained from the simulations. Here, the forces are calculated as the time average at fixed star centers. The drag force is always repulsive; it is positive for $\Delta x < 0$ and negative for $\Delta x > 0$ (Fig. 1).

A star dragged in a fluid experiences Stokes friction by the solvent, as is evident in Fig. 2 at small and large Δx, where the two stars do not overlap. It is proportional to the drag velocity. At large drag velocities—note that only the central particle experiences an external force—a star undergoes conformational changes. However, we apply sufficiently small external forces such that the spherical symmetry is only weakly perturbed.

When the arms of the two stars start to interact with each other while being dragged, $\Delta x/R_g \gtrsim -3$, the repulsive forces increase somewhat stronger than the equilibrium values (Fig. 2). At the same time, the position of the maximum moves to larger Δx with increasing drag velocity. More importantly, the force-distance curve exhibits a qualitative different behavior for large Pe at $\Delta x > 0$; here, the force is always positive, which implies that the stars exhibit an apparent attraction.

The total force on a star $\boldsymbol{F} = \boldsymbol{F}_{\mathrm{LJ}} + \boldsymbol{F}_f$ comprises contributions from direct intermolecular interactions due to excluded volume interactions ($\boldsymbol{F}_{\mathrm{LJ}}$), the dominant

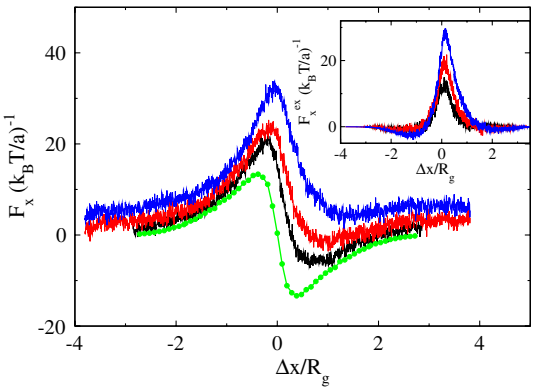

FIG. 2 (color online). Drag forces for the Peclet numbers $\mathrm{Pe} = v_d\tau_r/R_g = 0$ (green, bottom curve), 0.3 (black curve), 0.7 (red curve), and 1.3 (blue, top curve). The distance is $R_d/R_g = 0.48$ and $f = 40$. The inset shows the corresponding excess forces, i.e., the differences between the intermolecular forces at nonzero Pe and the equilibrium forces.

contribution, and interactions mediated by the solvent ($\boldsymbol{F}_f$). The solvent interactions themselves include contributions from Stokes friction, as mentioned above, and hydrodynamic interactions. The additional force is due to the flow field induced by a dragged object and effects the dynamics of the other colloid [15]. These hydrodynamic interactions are almost negligible at large separations. As the relative separation is comparable with the radius of gyration, the interactions increase and reach a maximum at the minimum center-center separation. Here, the force magnitude is on the order of that of Stokes friction. The inset of Fig. 2 shows the excess intermolecular forces $F_x^{\mathrm{ex}} = F_{x,\mathrm{LJ}} - F_{x,\mathrm{LJ}}^0$, where $\boldsymbol{F}_{\mathrm{LJ}}^0$ is the Lennard-Jones force at equilibrium. It clearly demonstrates that the dominant nonequilibrium contribution is an attractive force for $\Delta x > 0$, which increases rapidly with increasing drag velocity.

We characterize the shape of a star polymer by the radius-of-gyration tensor

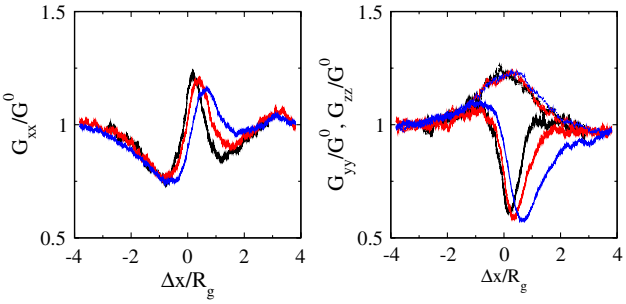

FIG. 3 (color online). Gyration tensor components along (G_{xx}, left) and perpendicular (G_{yy}, G_{zz}, right) to the drag direction for the Peclet numbers $\mathrm{Pe} = 0.3$ (black curve), 0.7 (red [medium gray] curve), and 1.3 (blue [dark gray] curve). The distance is $R_d/R_g = 0.48$ and $f = 40$.

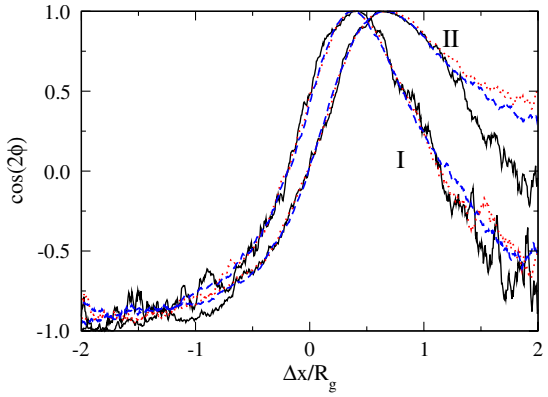

FIG. 4 (color online). Alignment angle ϕ as a function of functionality and drag velocity. Set I of curves is for $f = 20$ (solid line), $v_d = v_d^0$; $f = 40$ (dashed line), $v_d = 2v_d^0$; $f = 60$ (dotted line), $v_d = 3v_d^0$, and set II for $f = 20$, $v_d = 2v_d^0$; $f = 40$, $v_d = 4v_d^0$; $f = 60$, $v_d = 6v_d^0$, where $v_d^0 = 2.5 \times 10^{-4}\sqrt{k_B T/m}$. The distance is $R_d/R_g = 0.48$.

$$G_{\alpha\beta} = \frac{1}{N}\sum_{i=1}^{N}\langle \Delta r_{i,\alpha}\Delta r_{i,\beta}\rangle, \tag{1}$$

where $N = fN_m + 1$ is the total number of monomers, $\Delta \boldsymbol{r}_i$ the position of monomer i in the center-of-mass reference frame, and $\alpha, \beta \in \{x, y, z\}$. At equilibrium, all diagonal components are equal to $G_{\alpha\alpha} = G^0 = R_g^2/3$. A scaling analysis of the radius of gyration suggests the dependence $R_g^2 \sim b^2 N_m^{2\nu} f^{1-\nu}$ on arm length and functionality [14]. Our simulation results agree with this prediction for $\nu = 0.63$.

At low Peclet numbers, $\mathrm{Pe} < 1$, the behavior of the stars, as reflected in the variation of $G_{\alpha\alpha}$ with Δx in Fig. 3, can be understood by an oblate deformation and simultaneous rotation of each star polymer. For Peclet numbers $\mathrm{Pe} \gtrsim 1$, G_{xx} and G_{yy} become asymmetric, reflecting the asymmetry in the force curves (Fig. 2), and larger Peclet numbers lead to larger shape asymmetries. Interestingly, G_{zz} increases in response to the arm overlap, however, it is almost independent of Pe.

Star rotation during dragging is measured by the angle ϕ between the main axis of the gyration tensor and the dragging direction, defined as

$$\cos(2\phi) = \frac{G_{xx} - G_{yy}}{\sqrt{4G_{xy}^2 + (G_{xx} - G_{yy})^2}}. \tag{2}$$

At weak encounter, the main axis of an oblate star is mainly in the xy plane, which corresponds to $\cos(2\phi) \approx -1$. With increasing Δx, the deformed stars rotate and at $\Delta x = 0$, the main axis is almost parallel to the dragging direction. During departure, the alignment angle traverses a similar sequence and $\cos(2\phi)$ reaches almost the same minimal value at $\Delta x/R_g \approx 2$. A larger drag velocity yields a shift of the position, where $\cos(2\phi) = 1$ toward larger Δx, consistent with the conformational changes (Fig. 3). Interestingly, stars of different functionality follow the same sequence of alignment angles at corresponding drag velocities. This is shown in Fig. 4 for two sequences of drag velocities. Increasing the functionality by two and three and increasing the drag velocity by the same factors yields almost the same curves. This suggests that over a certain range of separations Δx, the alignment angle follows the scaling relation

$$\cos(2\phi) = \mathcal{F}(\mathrm{Pe}/f^{(1+\nu)/2}), \tag{3}$$

where $\mathrm{Pe}/f^{(1+\nu)/2} \sim v_d/f$.

The time-dependent overall shape of a star is illustrated by the monomer distributions for various star separations in Fig. 5. Monomers are shown within a slice of width $\pm 4a$ parallel to the xy plane and projected onto the that plane. During the approach of the stars, the arms toward the right are strongly compressed and/or the orientation is changed [Fig. 5(a)]. There seems to be hardly any polymer overlap between the stars in that region. At minimal separation, for $\Delta x = 0$, the monomer distribution is evidently far from symmetric with respect to the y axis [Fig. 5(b)]. We find an

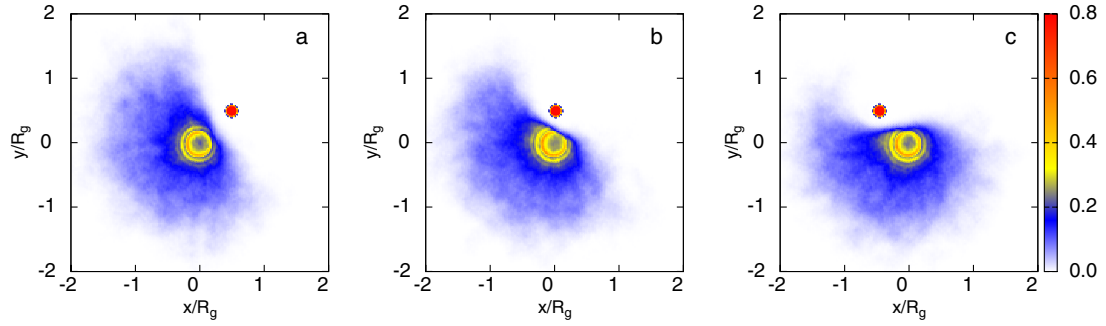

FIG. 5 (color online). Monomer density distributions within a slab of $\pm 4a$ parallel to the xy plane for $\mathrm{Pe} = 1.3$, $R_d/R_g = 0.48$, and the center separations $\Delta x/R_g = 0.48$ (a), 0 (b), and -0.48 (c). The (red) bullet indicates the center of the second star. See also movie S3 in the Supplemental Material [23].

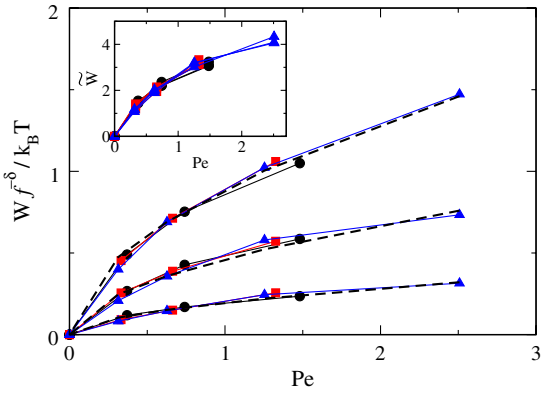

FIG. 6 (color online). Mechanical work as a function of drag velocity for the distances $R_d/R_g = 0.48$ (top lines), 0.76 (middle lines), and 1.14 (bottom lines), and functionalities $f = 20$ (●), 40 (■), and 60 (▲). The inset shows $\tilde{W} = W/(k_B T f^{\delta} e^{-\kappa R_d/R_g}) \sim \mathrm{Pe}^{\mu}$, with $\mu \approx 0.54$, $\kappa \approx 2.25$, and $\delta \approx 1.05$. The dashed lines are calculated according to Eq. (5).

increased monomer concentration for $x/R_g < 0.5$ and a reduced concentration for $x/R_g > 0.5$. The monomers for $x/R_g < 0.5$ act as a barrier for the star moving from right to left. Since the other star shows the same distribution, its monomers at $x/R_g > 0.5$ also act as a barrier. Finally, on departure, the degree of asymmetry is enhanced and an even more pronounced barrier is present [Fig. 5(c)]. Figures 5(a) and 5(c) correspond to the same separation, but due to the slow polymer dynamics the distributions are completely different. At equilibrium, these distributions would be mirror images of each other.

Symmetry breaking in the monomer distributions during the dragging process explains the appearance of the apparent star attraction. Since the Peclet number $\mathrm{Pe} = 1.3$ is larger than unity, the polymer arms are unable to relax while the two stars move past each other. In turn, this implies that drag-induced monomer density inhomogeneities are unable to relax and act as temporary barriers. Thus, the apparent attraction is a consequence of the "retarded relaxation" of the nonequilibrium process.

Energy is dissipated during the (isothermal) dragging process. In the quasistatic limit, the force-distance curve is antisymmetric and, hence, the total work

$$W = \int_C \boldsymbol{F}_{\mathrm{LJ}} d\boldsymbol{r} \tag{4}$$

is zero. This changes at finite Peclet numbers and W increases with increasing Pe as shown in Fig. 6. The dependence on functionality f, distance R_d/R_g, and Peclet number Pe is well described by the expression

$$W/k_B T \sim f^{\delta} \mathrm{Pe}^{\mu} e^{-\kappa R_d/R_g}, \tag{5}$$

with $\mu \approx 0.54$, $\kappa \approx 2.25$, and $\delta \approx 1.05$, as shown in Fig. 6. There is a surprisingly strong (exponential) dependence on the distance between the stars and a square-root dependence on the Peclet number only. Further theoretical studies are necessary to explain the observed functional dependencies.

Various interaction mechanisms may determine the friction between star polymers sliding past each other. Here, we have shown that monomer repulsion suppresses chain interpenetration, and symmetry breaking of monomer density distribution provides time irreversibility and energy dissipation. In contrast, in Refs. [9,22], overlapping coronas and resulting entanglements among the arms of different polymers are assumed and discussed as a fundamental interaction mechanism. This type of interaction does not play a significant role for our stars with relatively short arm lengths, because the time required to form entanglements is too long compared to the passing time τ_d for the velocities needed to observe attraction. An important question for future studies is the relevance of polymer arm length for the friction mechanism.

Financial support by the German Research Foundation (DFG) within SFB TR6 is gratefully acknowledged.

[1] J. Klein, E. Kumacheva, D. Mahula, D. Perahia, and L. J. Fetters, Nature (London) **370**, 634 (1994).
[2] B. N. J. Persson, *Sliding Friction: Physical Principles and Applications* (Springer, Berlin, 2000).
[3] M. H. Müser, M. Urbakh, and M. O. Robbins, Adv. Chem. Phys. **126**, 187 (2003).
[4] H. A. Stone, Annu. Rev. Fluid Mech. **26**, 65 (1994).
[5] V. Sibillo, G. Pasquariello, M. Simeone, V. Cristini, and S. Guido, Phys. Rev. Lett. **97**, 054502 (2006).
[6] V. Kantsler and V. Steinberg, Phys. Rev. Lett. **95**, 258101 (2005).
[7] H. Noguchi and G. Gompper, Proc. Natl. Acad. Sci. U.S.A. **102**, 14159 (2005).
[8] K. Kegler, M. Salomo, and F. Kremer, Phys. Rev. Lett. **98**, 058304 (2007).
[9] W. J. Briels, Soft Matter **5**, 4401 (2009).
[10] D. Vlassopoulos and G. Fytas, Adv. Polym. Sci. **236**, 1 (2010).
[11] B. M. Erwin, M. Cloitre, M. Gauthier, and D. Vlassopoulos, Soft Matter **6**, 2825 (2010).
[12] J. K. G. Dhont and W. J. Briels, Rheol. Acta **47**, 257 (2008).
[13] C. N. Likos, H. Löwen, M. Watzlawek, B. Abbas, O. Jucknischke, J. Allgaier, and D. Richter, Phys. Rev. Lett. **80**, 4450 (1998).
[14] C. N. Likos, Phys. Rep. **348**, 267 (2001).
[15] J. M. D. Lane, A. E. Ismail, M. Chandross, C. D. Lorenz, and G. S. Grest, Phys. Rev. E **79**, 050501(R) (2009).
[16] Y. Min, M. Akbulut, K. Kristiansen, Y. Golan, and J. Israelachvili, Nature Mater. **7**, 527 (2008).

[17] A. Malevanets and R. Kapral, J. Chem. Phys. **110**, 8605 (1999).
[18] R. Kapral, Adv. Chem. Phys. **140**, 89 (2008).
[19] G. Gompper, T. Ihle, D. M. Kroll, and R. G. Winkler, Adv. Polym. Sci. **221**, 1 (2009).
[20] C.-C. Huang, R. G. Winkler, G. Sutmann, and G. Gompper, Macromolecules **43**, 10107 (2010).
[21] M. Ripoll, R. G. Winkler, and G. Gompper, Phys. Rev. Lett. **96**, 188302 (2006).
[22] W. J. Briels, D. Vlassopoulos, K. Kang, and J. K. G. Dhont, J. Chem. Phys. **134**, 124901 (2011).
[23] See Supplemental Material at http://link.aps.org/supplemental/10.1103/PhysRevLett.107.158301 for simulation animations.